



Thickness-tunable polyimide nanoencapsulating layers and their influence on cell performance/thermal stability of high-voltage LiCoO_2 cathode materials for lithium-ion batteries

Jang-Hoon Park^a, Ju-Hyun Cho^a, Eun-Ho Lee^a, Ju-Myung Kim^a, Sang-Young Lee^{b,*}

^a Department of Chemical Engineering, Kangwon National University, Chuncheon, Kangwondo 200-701, Republic of Korea

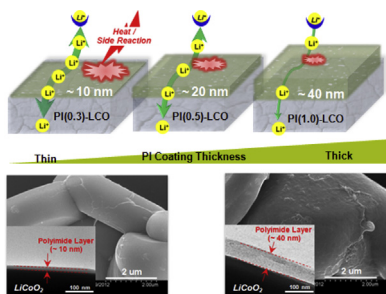
^b Interdisciplinary School of Green Energy, Ulsan National Institute of Science and Technology (UNIST), Ulsan 689-798, Republic of Korea



HIGHLIGHTS

- Thickness-tunable polyimide nanoencapsulating layer is introduced on LiCoO_2 surface.
- Effect of PI coating thickness on high-voltage cell performance is explored.
- PI encapsulating layer is featured with nanometer-thick, large surface coverage.
- PI coating thickness of 10 nm imparts well-balanced coating effects on 4.4 V LiCoO_2 .
- Beneficial coating effects can be optimized by tuning PI coating thickness.

GRAPHICAL ABSTRACT



ARTICLE INFO

Article history:

Received 20 October 2012

Received in revised form

25 November 2012

Accepted 26 November 2012

Available online 5 December 2012

Keywords:

Lithium-ion batteries

High-voltage cathode materials

Surface modification

Polyimide

Encapsulating layers

Coating thickness

ABSTRACT

We have previously demonstrated polyimide (PI) gel polymer electrolyte (GPE)-based nanoencapsulation as a new surface modification strategy for high-voltage cathode materials. In this study, in an endeavor to attain a more comprehensive understanding of the PI GPE-based surface modification, effects of structural variation of PI encapsulating layers (specifically, focusing on PI coating thickness) on cell performance and thermal stability of high-voltage (4.4 V) LiCoO_2 are investigated. Herein, PI coating thickness is tuned between approximately 10 and 40 nm by varying polyamic acid (synthesized from pyromellitic dianhydride/oxydianiline) concentration of coating solutions. As PI coating thickness is increased, discharge C-rate capability of cells is deteriorated due to undesired rise of ionic and electronic resistance of thick PI coating layers. On the other hand, thick PI encapsulating layers are effective in mitigating interfacial exothermic reaction between delithiated LiCoO_2 and liquid electrolyte. Notably, among the various PI coating thicknesses, average thickness of 10 nm imparts well-balanced enhancement in cell performance and thermal stability. These results demonstrate that structural fine-tuning (particularly, coating thickness) of PI encapsulating layers, acting as ion-conductive protective conformal thin films, plays a significant role in optimizing their beneficial coating effects on high voltage LiCoO_2 .

© 2012 Elsevier B.V. All rights reserved.

* Corresponding author. Tel.: +82 33 250 6338; fax: +82 33 251 3658.

E-mail address: sangyounglee87@gmail.com (S.-Y. Lee).

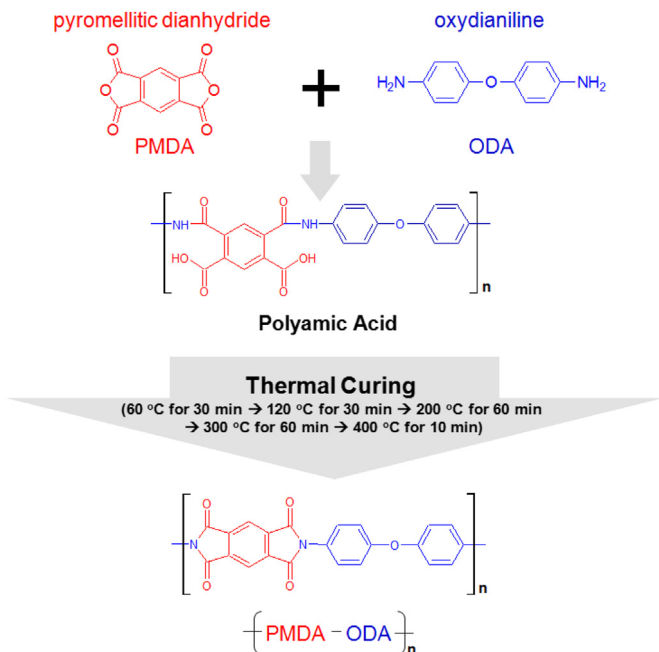


Fig. 1. Chemical structures of pyromellitic dianhydride (PMDA)/oxydianiline (ODA) polyamic acid and resulting polyimide (PI). Detailed information on a stepwise imidization process is also provided.

1. Introduction

As applications of lithium-ion batteries are vigorously expanding into newly emerging fields such as (hybrid) electric vehicles and power grids, development of new cathode active materials capable of offering large reversible capacity is strongly demanded [1–5]. Among various cathode materials, LiCoO₂ (LCO) has been most widely used in commercial lithium-ion batteries owing to the ease of manufacturing procedure and well-balanced electrochemical performance. Meanwhile, in an effort to increase the capacity of LCO, charging cells above a conventional cut-off voltage of 4.2 V has been extensively investigated [6–10]. However, raising the charge cut-off voltage entails confronting formidable challenges related to deterioration of cell performance (particularly, cyclability) and thermal stability. These problems are mainly due to undesirable interfacial side reactions between the delithiated LCO and liquid electrolytes, where liquid electrolytes are highly prone to electrochemical decomposition at high voltage conditions. Hence, it is no doubt that interfacial control between the LCO and liquid electrolyte is crucially important in the development of high-voltage cells.

One promising attempt to resolve these challenges of the high-voltage LCO is the surface modification of LCO with inorganic materials such as Al₂O₃ [8,9], ZrO₂ [10], ZnO [11], AlPO₄ [12], and AlF₃ [13,14]. Unfortunately, these inorganic materials, although they are effective in suppressing the interfacial side reactions, tend to be discontinuously deposited on LCO surface and behave as an

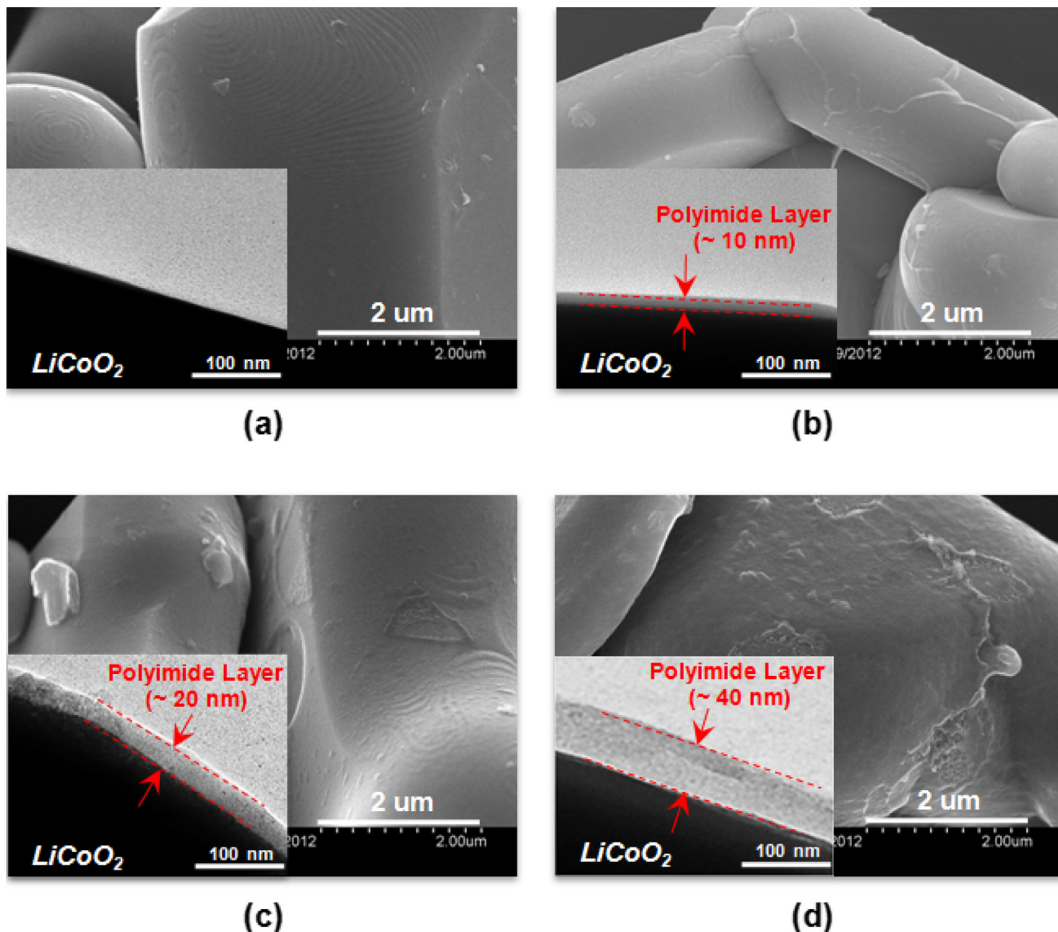


Fig. 2. FE-SEM photographs of: (a) pristine LCO; (b) PI(0.3)-LCO; (c) PI(0.5)-LCO; (d) PI(1.0)-LCO. Insets are TEM photographs of pristine LCO and various PI-LCO samples.

inert layer hampering ionic and electronic transport. In addition, they often require complex and cost-consuming coating processes.

As a new surface-modification approach to overcome the stringent shortcomings of the inorganic material coatings, the polyimide (PI) gel polymer electrolyte (GPE)-based nano-encapsulation was reported in our previous studies [15–17]. The PI encapsulating layers were featured with nanometer-thick, highly-continuous surface coverage and provision of facile ion transport.

In the present study, in an endeavor to attain a more comprehensive understanding of the abovementioned PI GPE-based surface modification, effects of structural variation of PI encapsulating layers (specifically, focusing on PI coating thickness) on cell performance and thermal stability of high-voltage (herein, 4.4 V) LCO are systematically investigated. The PI encapsulating layers are introduced on LCO surface via thermal imidization of polyamic acid copolymers synthesized from pyromellitic dianhydride (PMDA)/oxydianiline (ODA). The PI coating thickness is fine-tuned by varying the polyamic acid concentration of coating solutions. Morphological features of the PI-encapsulated LCO (hereinafter, referred to as “PI-LCO”) are characterized as a function of PI coating thickness. Based on the structural characterization of thickness-tunable PI encapsulating layers, their influence on high-voltage cell performance (including discharge capacity, C-rate capability, and cyclability) and interfacial exothermic reaction between

delithiated LCO and liquid electrolytes is scrutinized and discussed with an in-depth consideration of the unique structure of ion-conductive protective conformal PI thin films.

2. Experimental

2.1. Fabrication of PI-encapsulated LCO with varied coating thickness

The PMDA/ODA polyamic acid coating solutions were prepared using dimethyl acetamide (DMAc) as a solvent under a nitrogen atmosphere (Fig. 1). The molar ratio of PMDA/ODA in the coating solutions was 1.00/1.01. The detailed synthesis and characterization of the polyamic acid have been described in previous studies [18–20]. LCO powders (average particle size = 5 μm, Daejung EM) were added into the polyamic acid solutions and then were subjected to vigorous mixing for 1 h. Here, in order to fine-tune the thickness of polyamic acid coating layers on LCO surface, the polyamic acid concentrations in the coating solutions were varied as 0.3 (denoted as “PI(0.3)-LCO”), 0.5 (“PI(0.5)-LCO”), and 1.0 wt% (“PI(1.0)-LCO”), respectively. Subsequently, the LCO powders were filtered from the polyamic acid solutions and vacuum-dried at 30 °C for 4 h. Meanwhile, in order to convert the polyamic acid into the PI, the polyamic acid-coated LCO powders were thermally cured via a stepwise imidization process (60 °C for 30 min → 120 °C for

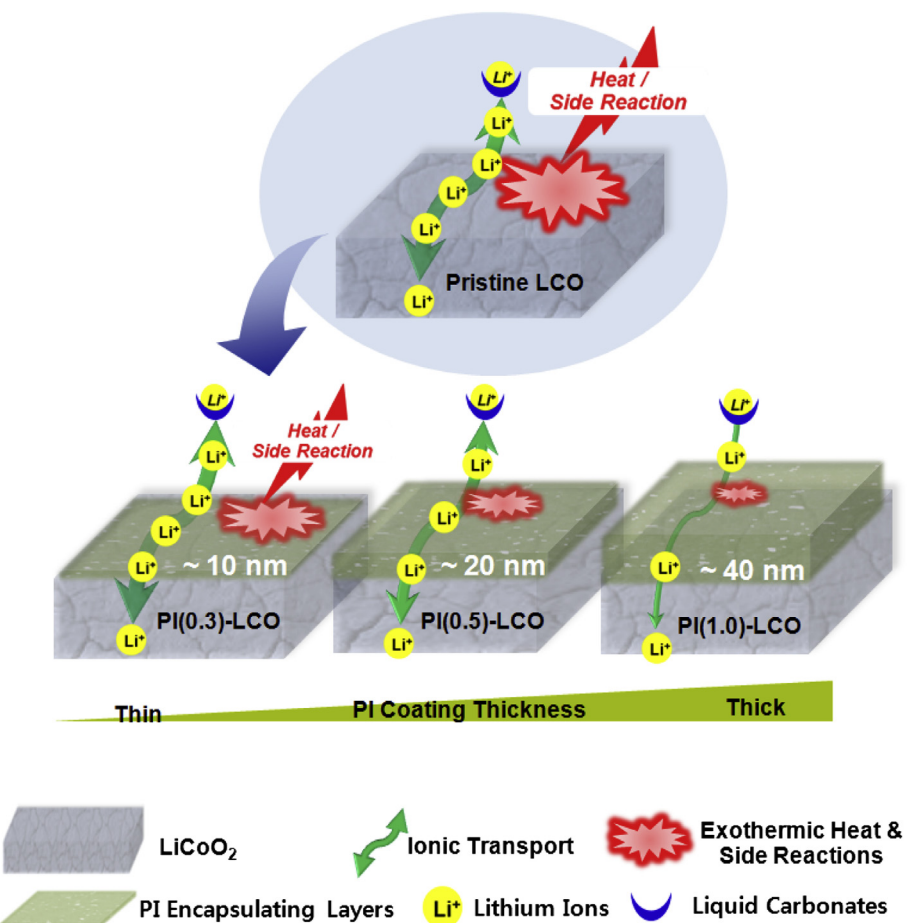


Fig. 3. Schematic representations illustrating PI coating thickness variation and its influence on ionic conductance and interfacial side reactions between LCO and liquid electrolytes. Advantageous effects of PI encapsulating layers (as an unusual ion-conductive protective conformal thin film) on the suppression of unwanted interfacial side reactions are also depicted.

30 min → 200 °C for 60 min → 300 °C for 60 min → 400 °C for 10 min) under a nitrogen atmosphere (Fig. 1).

2.2. Structural characterization of PI encapsulating layers and cell performance/thermal stability of PI-encapsulated LCO

The surface morphology of the PI-LCO was examined using a field emission scanning electron microscope (FE-SEM, S-4800, Hitachi) and a transmission electron microscope (TEM, JEM-2010, JEOL). The crystalline phase of the PI-LCO was analyzed with a powder X-ray diffractometer (XRD, PANalytical, MPD) using Cu K α radiation between 10 and 80° at a scan rate of 0.01° s $^{-1}$. The imidization reaction of the polyamic acid was confirmed using a FT-IR spectrometer (FT-3000, Excalibur) by observing the characteristic peaks assigned to the imide ring of the PI coating layers [15–17]. LCO cathodes were fabricated by coating a NMP-based slurry with a mixture of 95 wt% of LCO, 3 wt% of polyvinylidene fluoride (PVdF) binder, and 2 wt% of carbon black on an aluminum current collector. A unit cell (2032-type coin) was assembled by sandwiching a PE separator (thickness = 20 μ m, Tonen) between a natural graphite anode (natural graphite (average particle size = 20 μ m, Sodiff)/CMC/SBR = 97.5/1.0/1.5 w/w/w) and the PI-LCO cathode. The unit cell was then activated by being filled with a liquid electrolyte of 1 M LiPF₆ in ethylene carbonate (EC)/ethyl methyl carbonate (EMC) (=1/2 v/v, Soulbrain). The cell performance including discharge capacity, C-rate capability, and cyclability was examined using battery test equipment (PNE Solution). The discharge capacities and C-rate capability were evaluated by varying discharge current densities (i.e., discharge C-rates) from 0.2 (=0.52 mA cm $^{-2}$) to 2.0 C (=5.23 mA cm $^{-2}$) at a constant charge current density of 0.2 C under a voltage range of 3.0–4.4 V. The cells were cycled at a constant charge/discharge current density of 0.5 C/0.5 C. The AC impedance of the cells was measured using an impedance analyzer (VSP classic, Bio-Logic) over a frequency range of 10 $^{-3}$ to 10 6 Hz. The interfacial exothermic reaction between the delithiated LCO and liquid electrolyte was examined by differential scanning calorimetry (DSC, DuPont Q2000) measurements, where the cells were charged to 4.4 V at a current density of 0.1 C and then disassembled in a dry room to remove the charged cathode. The DSC measurements were performed in a temperature range from room temperature to 350 °C at a heating rate of 10 °C min $^{-1}$ under a nitrogen atmosphere.

3. Results and discussion

3.1. Structural characterization of PI-encapsulated LCO (PI-LCO)

Firstly, structural characterization of PI-LCO was conducted as a function of PI coating thickness. Fig. 2 shows that, in comparison to the pristine LCO with smooth planes and well-defined edges, the PI-LCO is characterized with extremely thin and highly continuous PI coating layers, although perfect surface coverage is not achieved. It has been reported that the polyamic acid (a precursor polymer of the resulting PI) shows high polarity [20], which may allow strong affinity for LCO. This benign compatibility of the polyamic acid toward LCO, in combination with its outstanding film-forming capability [18–20], may contribute to the facile formation of the nanostructured PI encapsulating layers on LCO surface. This morphological uniqueness of the PI-LCO is a distinctive feature, as compared to conventional inorganic material coatings yielding discontinuously deposited, ionically-inert layers [8–14].

Unfortunately, from the FE-SEM results, it is difficult to clearly identify the morphological difference between the various PI-LCO samples. Hence, in order to provide more precise information about the PI encapsulating layers, the TEM characterization of

PI-LCO was accompanied. Insets of Fig. 2 exhibit that the LCO is well covered with ultrathin, conformal PI coating layers. A notable finding is that, as the polyamic acid concentration of coating solutions increases from 0.3 to 1.0 wt%, the PI coating thickness becomes larger (i.e., PI coating thickness: ~10 nm at PI(0.3)-LCO → ~40 nm at PI(1.0)-LCO), although some thickness fluctuations are observed. This morphological analysis demonstrates that the PI coating thickness can be easily tuned in the nanometer regime by varying the polyamic acid concentration of coating solutions. The effects of coating thickness variation on ionic conductance of PI coating layers and interfacial side reactions between the LCO and liquid electrolytes, which will be discussed more in the following section, are schematically illustrated in Fig. 3.

The XRD patterns of the PI-LCO were compared with those of the pristine LCO in Fig. 4(a). The well-defined hexagonal layered structure with space group of R $\bar{3}m$ [14,21,22] is observed in the PI-LCO as well as the pristine LCO. No significant crystallographic difference in the XRD patterns was detected between the pristine LCO and PI-LCO. The lattice parameters of the LCO samples were calculated by the Rietveld refinement of the XRD results. The

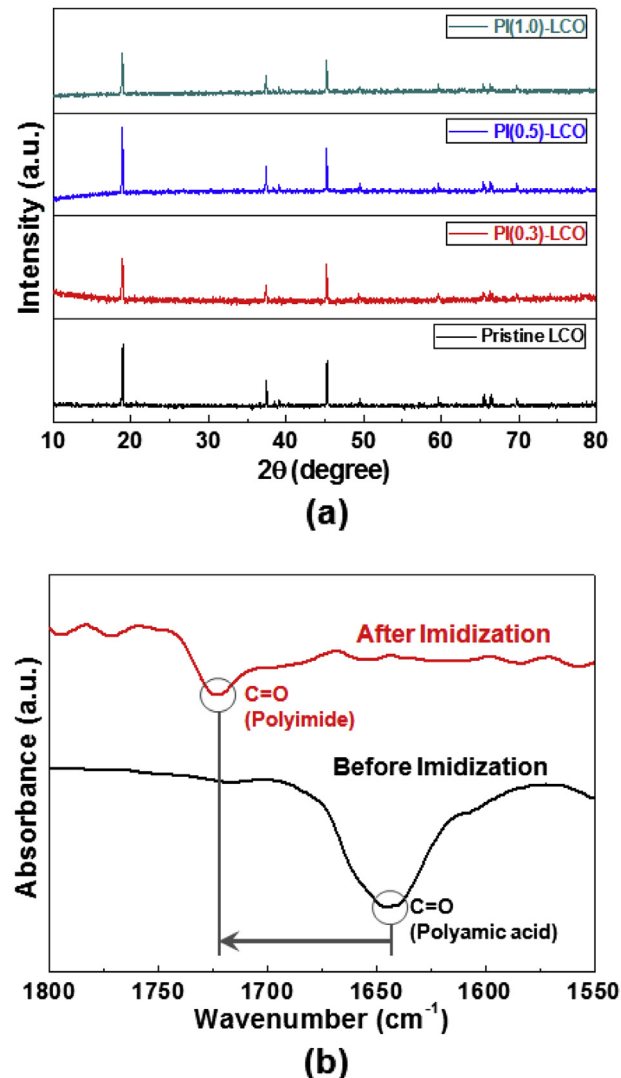


Fig. 4. (a) XRD patterns of pristine LCO and PI-LCO as a function of PI coating thickness. (b) FT-IR spectra of PI(0.3)-LCO, where the characteristic peak assigned to the C=O bond shifts from 1650 cm $^{-1}$ (starting polyamic acid) to 1723 cm $^{-1}$ (resulting PI coating layer).

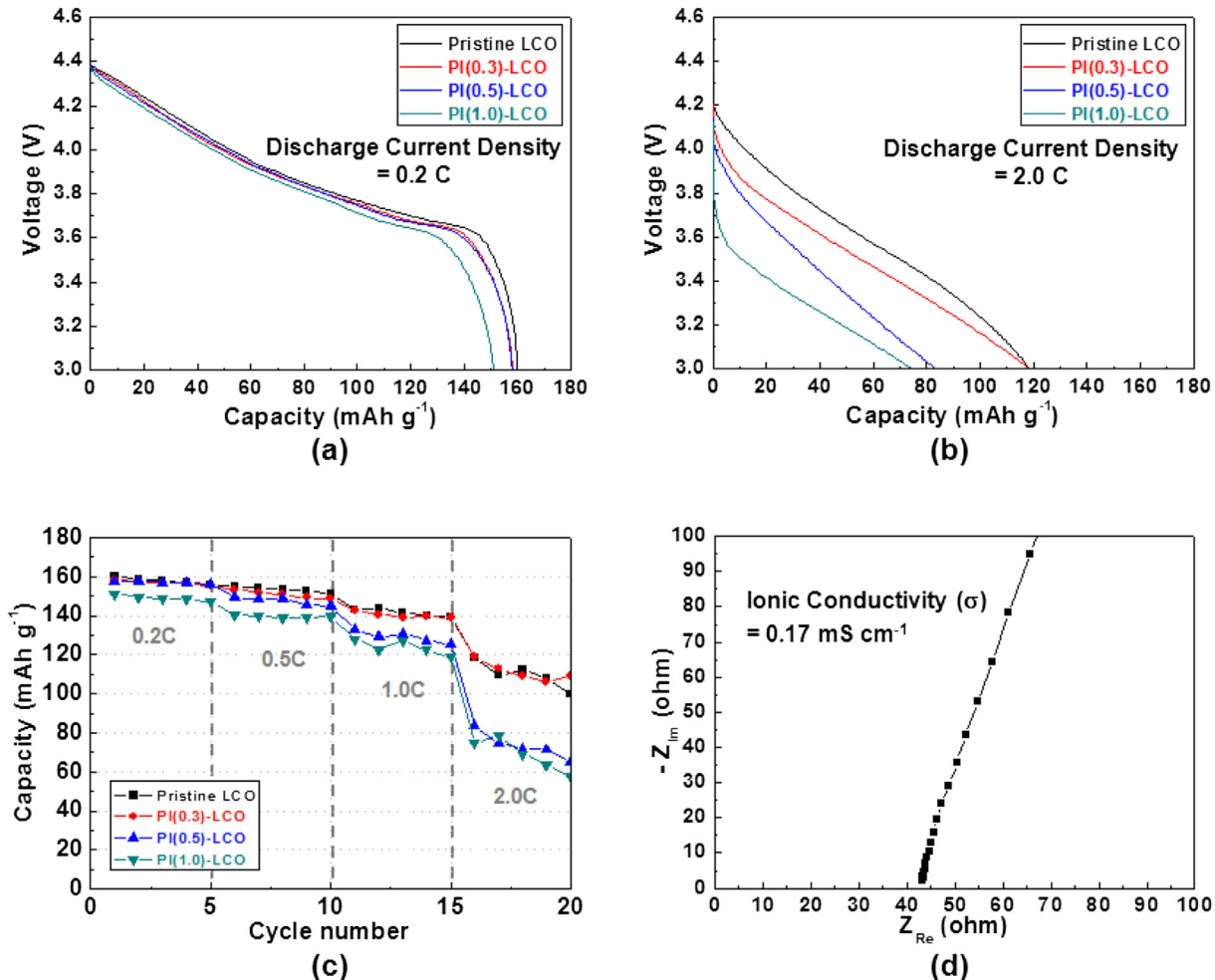


Fig. 5. Discharge profiles of cells assembled with pristine LCO or PI-LCO: (a) at discharge current density = 0.2 C; (b) at discharge current density = 2.0 C, where the discharge capacities are measured at a constant charge current density of 0.2 C under a voltage range of 3.0–4.4 V. (c) Comparison of discharge C-rate capability between pristine LCO and PI-LCO. (d) AC impedance spectrum for estimating ionic conductivities of a PI film swelled with liquid electrolyte (1 M LiPF₆ in EC/EMC = 1/2 v/v).

calculated lattice parameters of the PI-LCO are very similar to those of the pristine LCO. More importantly, they are negligibly influenced by the coating thickness variation. For example, the lattice parameters of the pristine LCO and PI-LCO are, respectively, $a = 2.8151 \text{ \AA}$, $c = 14.03 \text{ \AA}$ for pristine LCO; $a = 2.8151 \text{ \AA}$, $c = 14.03 \text{ \AA}$ for PI(0.3)-LCO; $a = 2.8170 \text{ \AA}$, $c = 14.04 \text{ \AA}$ for PI(0.5)-LCO; $a = 2.8170 \text{ \AA}$, $c = 14.03 \text{ \AA}$ for PI(1.0)-LCO. This quantitative characterization of XRD patterns demonstrates that the introduction of PI encapsulating layers, regardless of PI coating thickness, does not disrupt the typical layered crystalline structure of LCO.

In addition, the chemical structure of PI encapsulating layers was characterized by carrying out FT-IR measurements, where the PI(0.3)-LCO was chosen as a representative sample. Fig. 4(b) shows that the FT-IR peak attributed to the C=O bonds of the PI encapsulating layer is observed at 1723 cm⁻¹, whereas the starting polyamic acid presents the peak of the C=O bond at 1650 cm⁻¹. This shift in the characteristic peak of the C=O bonds verifies that the polyamic acid is successfully imidized on the LCO surface, leading to the PI coating layer.

3.2. High-voltage cell performance and thermal stability of PI-encapsulated LCO (PI-LCO)

The effect of PI-LCO on high-voltage (herein, 4.4 V) cell performance was investigated as a function of PI coating thickness. Fig. 5

shows the discharge capacities and discharge C-rate capability of cells, where the discharge current densities were varied from 0.2 to 2.0 C at a constant charge current density of 0.2 C. No abnormal or unstable discharge profiles were observed at the pristine LCO and also PI-LCO. An intriguing finding is that the discharge capacities of PI-LCO are influenced by the PI coating thickness. Fig. 5(a) shows that, at a low discharge current density of 0.2 C, the discharge capacity of PI(0.3)-LCO with a coating thickness of ~10 nm is almost comparable to that of pristine LCO. On the other hand, for the PI(1.0)-LCO with a coating thickness of approximately 40 nm, the discharge capacity is decreased to ~150 mA h g⁻¹. This dependence of discharge capacity on PI coating thickness is further examined at a higher discharge current density of 2.0 C. Fig. 5(b) presents that the discharge capacity of PI-LCO with the thick coating layers decreases more drastically (~119 mA h g⁻¹ for the pristine LCO vs. ~73 mA h g⁻¹ for the PI(1.0)-LCO). Fig. 5(c) summarizes the discharge C-rate capability of PI-LCO as a function of PI coating thickness. Except for the PI(0.3)-LCO with relatively thin coating thickness, other PI-LCO samples present the lower discharge C-rate capability than the pristine LCO.

This discharge C-rate capability behavior of the PI-LCO samples can be explained by considering actual ionic conductance of the PI coating layers. Herein, a supplementary experiment for evaluating ionic conductivity of a PI thin film swelled with the liquid electrolyte (1 M LiPF₆ in EC/EMC = 1/2 v/v) was carried out. The liquid

electrolyte-swollen PI film was observed to deliver a high ionic conductivity of 0.17 mS cm^{-1} at room temperature (Fig. 5(d)). Considering that ionic conductance ($=\sigma \times A \times L^{-1}$, where σ = ionic conductivity, A = film area, and L = film thickness) of a film is directly affected by its thickness, it can be expected that ionic conductance of PI encapsulating layers tends to decrease in proportion to the increment of PI coating thickness. Hence, for thick PI encapsulating layers, low ionic conductance (i.e., high ionic resistance) is observed, causing an appreciable rise in the ohmic polarization (i.e., IR drop [23–25]) of cells, which becomes more serious at higher discharge current densities. In comparison, ionic transport via thin PI encapsulating layers is likely to be insignificantly impeded due to relatively short diffusion pathways of lithium ions. This strong dependence of ionic conductance on the PI coating thickness is conceptually illustrated in Fig. 3.

In addition to the abovementioned ionic conductance, another important factor to affect the discharge C-rate capability of cells is the (surface) electronic resistance of PI-LCO. The PI encapsulating layers, although they can show satisfactory ionic transport, are electronically inert. Therefore, it is reasonably speculated that electronic resistance of PI-LCO may be increased due to the presence of PI encapsulating layers and become higher with increasing PI coating thickness, possibly provoking additional rise of ohmic polarization. Fig. 5(b) verifies that the ohmic polarization of cells becomes pronounced as the PI encapsulating thickness is increased. The influence of PI encapsulating layers on ohmic polarization, which is combined output of ionic and electronic resistance, is further confirmed by measuring the initial AC impedance of cells (after 1st cycle). The insets of Fig. 7 show that, whereas the cell impedance ($Z_{\text{Re}} \sim 21 \Omega$) of the PI(0.3)-LCO is similar to that ($Z_{\text{Re}} \sim 20 \Omega$) of the pristine LCO, other PI-LCO samples having thicker PI encapsulating layers yield the higher cell impedances ($Z_{\text{Re}} \sim 31 \Omega$ at PI(0.5)-LCO, $Z_{\text{Re}} \sim 33 \Omega$ at PI(1.0)-LCO). A more detailed elucidation of the electronic resistance of PI-LCO and its influence on cell performance will be conducted in our future studies.

The effect of PI-LCO on the cycling performance (i.e., discharge capacity retention as a function of cycle number) of cells was investigated at a constant charge/discharge current density ($=0.5 \text{ C}/0.5 \text{ C}$). Fig. 6(a) shows that, at the high charge voltage of 4.4 V, the discharge capacity of pristine LCO sharply decreases, resulting in a very low discharge capacity of 110 mA h g^{-1} after 50th cycle. This poor cycling performance of pristine LCO may be attributed to its vigorous surface reactivity with liquid electrolyte. Previous studies [6–11] reported that, at high voltage conditions, liquid electrolytes are highly vulnerable to electrochemical decomposition on delithiated LCO surface, giving rise to the formation of unwanted resistive layers. The resistive layers may hamper charge transfer across LCO surface during cycling, which would consequently exert a negative influence on cycling performance of high-voltage charged cells.

In comparison, the PI-LCO shows the better cycling performance than the pristine LCO. In the very beginning of cycling, there is little difference in the discharge capacity between the pristine LCO and PI-LCO. However, as the cycle number is further increased, whereas the discharge capacity of pristine LCO continues to decline, the capacity fading of PI-LCO is substantially retarded at all PI encapsulating layers. Notably, the most stable capacity retention is observed at the PI(0.3)-LCO. After 50th cycle, the capacity retentions are found to be respectively 85% for PI(0.3)-LCO (vs. 71% for pristine LCO). Fig. 6(b) depicts the charge/discharge profiles (after 50th cycle) of cells, which underline that the ohmic polarization of cells is considerably mitigated in the PI-LCO, as compared to the pristine LCO. This improved cycling performance of PI-LCO underlines that the thickness-tunable PI encapsulating layers effectively

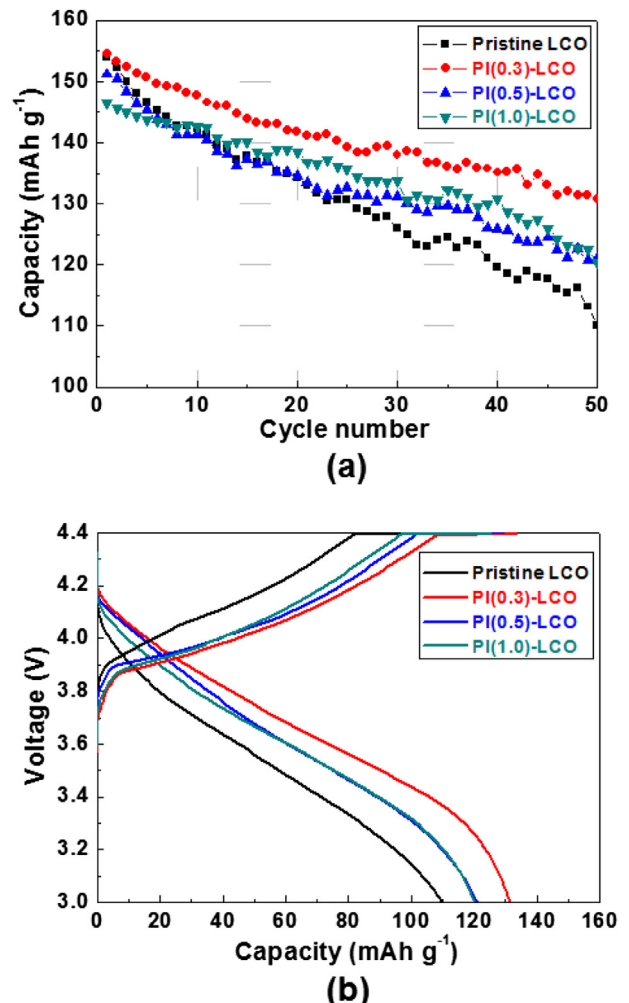


Fig. 6. (a) Cycling performance (at charge/discharge current density of 0.5 C/0.5 C and voltage range of 3.0–4.4 V) of cells assembled with pristine LCO or PI-LCO as a function of PI coating thickness. (b) Charge/discharge profiles of cells (after 50th cycle) assembled with pristine LCO or PI-LCO.

protect LCO surface from the attack of violent liquid electrolyte, which in turn suppresses the undesired interfacial side reactions between the LCO and liquid electrolyte. This advantageous effect of PI encapsulating layers (as a function of PI coating thickness) on the interfacial stability is schematically illustrated in Fig. 3.

In an effort to provide a more comprehensive understanding of the effect of PI-LCO on the cycling performance, the AC impedance spectra of 4.4 V-charged cells after 1st and 50th cycle were analyzed (Fig. 7). Previous studies [6–8,26,27] on a possible equivalent circuit of cells reported that the semicircle of impedance spectra at high frequency ranges represents the resistance of surface film formed on electrode materials and the semicircle observed at medium-to-low frequency regions is ascribed to charge transfer resistance between electrode materials and liquid electrolyte. Fig. 7(a) shows that the cell impedance of pristine LCO considerably increases after 50th cycle ($Z_{\text{Re}}(50\text{th cycle}) - Z_{\text{Re}}(1\text{st cycle}) = \Delta Z_{\text{Re}} \sim 260 \Omega$). This indicates that the sharp capacity fading of pristine LCO during the 4.4 V cycling is closely related to the formation of undesired resistive layers that may impede charge transfer via the interface between the LCO and liquid electrolyte, thus causing the continued increase of cell impedance.

On the other hand, for the PI-LCO, the growth of cell impedance after 50th cycle is considerably alleviated ($\Delta Z_{\text{Re}} \sim 70 \Omega$ at PI(0.3)-

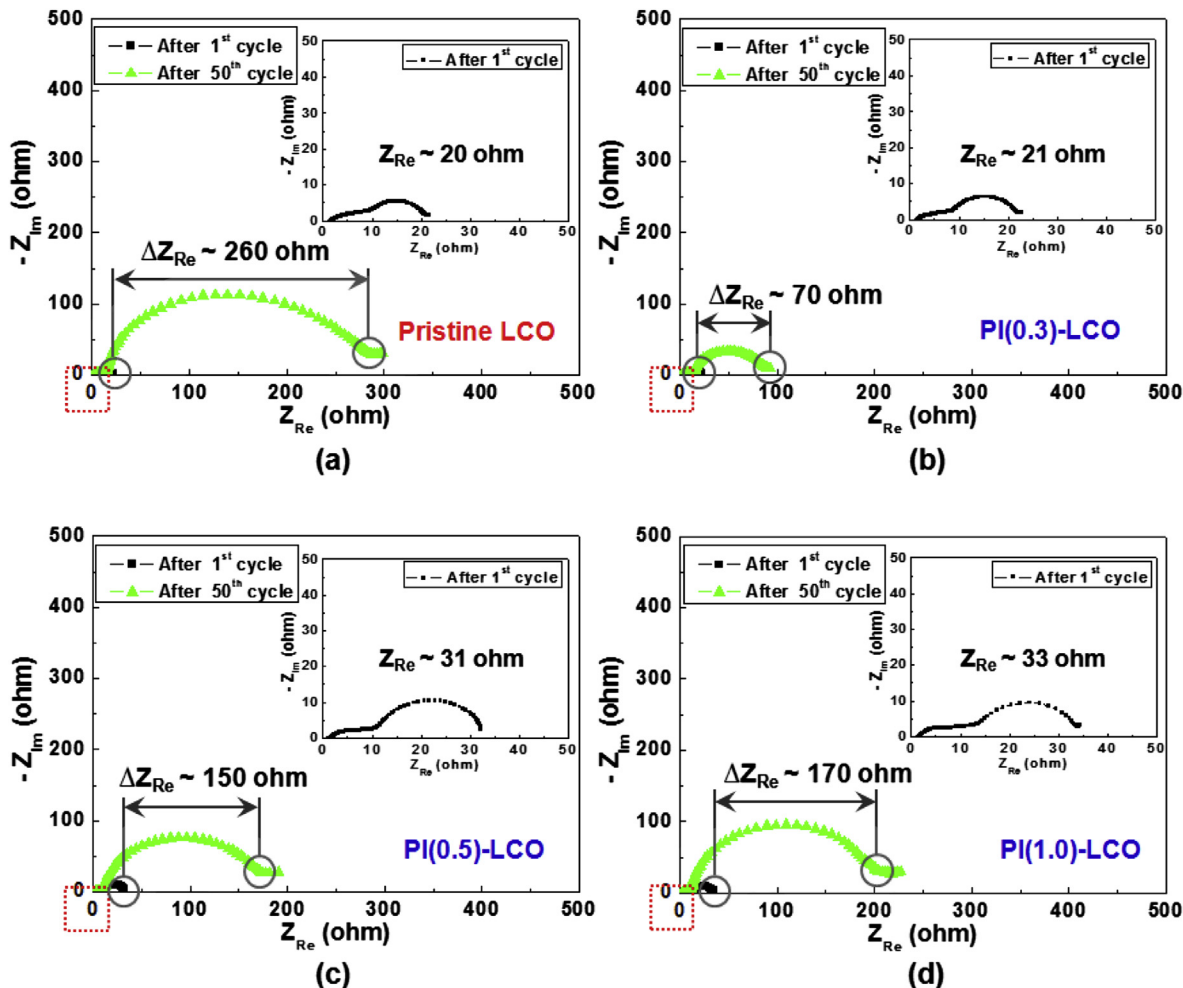


Fig. 7. Variation in AC impedance spectra (1st → 50th cycle) of cells: (a) pristine LCO; (b) PI(0.3)-LCO; (c) PI(0.5)-LCO; (d) PI(1.0)-LCO. Insets represent initial AC impedance spectra of cells after 1st cycle.

LCO, 150 Ω at PI(0.5)-LCO, 170 Ω at PI(1.0)-LCO), in comparison to that ($\Delta Z_{\text{Re}} \sim 260$ Ω) of the pristine LCO. This strongly supports that the PI encapsulating layers effectively prevent the direct exposure of charged LCO to liquid electrolyte during the high-voltage cycling. Hence, it is expected that the decomposition of liquid electrolyte on delithiated LCO surface is highly suppressed, contributing to the good capacity retention. More notably, among the PI-LCO samples, the PI(0.3)-LCO exhibits the lowest growth of cell impedance, which could be solid evidence for the superior cycling performance. The excellent cycling performance (Fig. 6), along with the discharge C-rate capability (Fig. 5), demonstrates that the PI encapsulating layer of PI(0.3)-LCO is well-tuned in terms of mitigating undesirable side reactions and also imparting facile ionic transport. Meanwhile, the relatively large increase in the impedance growth of the other PI-LCO samples (i.e., PI(0.5)-LCO and PI(1.0)-LCO), in comparison to that of the PI(0.3)-LCO, may be ascribed to the presence of thicker PI encapsulating layers, which give rise to long diffusion pathways of lithium ions and also impeded (surface) electron transport during cycling. This is also closely related to the larger ohmic polarization of the PI(0.5)-LCO (and PI(1.0)-LCO) in the charge/discharge profiles after 50th cycle (Fig. 6(b)), as compared to that of the PI(0.3)-LCO.

Finally, the effect of PI encapsulating layers on the thermal stability of 4.4 V-charged LCO was evaluated as a function of PI coating thickness. It has been already reported that, in the DSC results, reduction of total amount of heat generated by side reactions or shift of exothermic peak temperatures to higher values

indicates the thermally stabilized interface between electrode materials and liquid electrolytes [11–17]. Fig. 8 shows that the pristine LCO yields a large exothermic heat ($\Delta H = 706$ J g⁻¹) and low exothermic peak temperatures ($T_{\text{peak}} = 218, 243$ °C). This poor

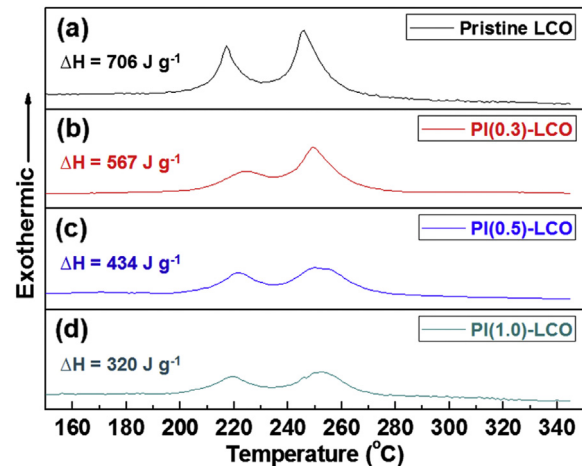


Fig. 8. DSC thermograms showing interfacial exothermic reaction between 4.4 V-charged LCO (or PI-LCO) and liquid electrolyte: (a) pristine LCO; (b) PI(0.3)-LCO; (c) PI(0.5)-LCO; (d) PI(1.0)-LCO.

thermal stability of the pristine LCO is attributed to the interfacial exothermic reaction of the delithiated LCO with liquid electrolyte.

In comparison, for the PI-LCO samples, the exothermic heat is considerably reduced and the exothermic peak shifts to a higher temperature. Interestingly, as the PI coating thickness is increased, the interfacial exothermic reaction between the delithiated LCO and liquid electrolyte is more alleviated (for example, $\Delta H = 567 \text{ J g}^{-1}$ for PI(0.3)-LCO vs. $\Delta H = 320 \text{ J g}^{-1}$ for PI(1.0)-LCO). These DSC results indicate that the PI encapsulating layers featuring nanometer-thick, highly-continuous surface coverage effectively prevent the LCO from coming into direct contact with violent liquid electrolyte. As a result, the interfacial exothermic reaction between the 4.4 V-charged PI-LCO and liquid electrolyte is mitigated. More notably, this improvement in thermal stability is more pronounced at thicker PI encapsulating layers. The improved thermal stability of PI-LCO and its strong dependence on the PI coating thickness is conceptually illustrated in Fig. 3.

4. Conclusion

The effects of structural variation (specifically, focusing on coating thickness) of PI encapsulating layers on the cell performance and thermal stability of high-voltage (4.4 V) LCO have been systematically investigated. The PI coating thickness was tuned between approximately 10 (PI(0.3)-LCO) to 40 nm (PI(1.0)-LCO) by varying the polyamic acid concentration of coating solutions. Among the various PI coating thicknesses examined in this study, the average thickness of 10 nm exhibited the well-balanced cell performance and thermal stability. As the PI coating thickness was increased, the ohmic polarization of cells became larger due to the unwanted rise of ionic and electronic resistance of the thick PI coating layers, which in turn exerted a detrimental influence on the discharge C-rate capability. Meanwhile, the PI-LCO samples presented the better cycling performance than the pristine LCO, notably the most stable capacity retention during cycling was observed at the PI(0.3)-LCO, which was further confirmed by the retarded growth of cell impedance. The interfacial exothermic reaction between the delithiated LCO and liquid electrolyte was substantially alleviated at the PI-LCO, which became more pronounced at the thicker PI encapsulating layers. In conclusion, the present study underlines that the beneficial effects of PI encapsulating layers (acting as ion-conductive protective

conformal thin films that suppress undesirable interfacial side reaction) on high-voltage LCO can be optimized by fine-tuning their coating architecture.

Acknowledgments

This research was supported by the Converging Research Center Program through the Ministry of Education, Science and Technology (2012K001254).

References

- [1] M.S. Whittingham, Chem. Rev. 104 (2004) 4271.
- [2] H. Li, Z. Wang, L. Chen, X. Huang, Adv. Mater. 21 (2009) 4593.
- [3] C. Liu, F. Li, L.P. Ma, H.M. Cheng, Adv. Mater. 22 (2010) E28.
- [4] J.B. Goodenough, Y. Kim, Chem. Mater. 22 (2010) 587.
- [5] B.L. Ellis, K.T. Lee, L.F. Nazar, Chem. Mater. 22 (2010) 691.
- [6] Z. Yang, W. Yang, D.G. Evans, G. Li, Y. Zhao, Electrochim. Commun. 10 (2008) 1136.
- [7] A. Abouimrane, I. Belharouak, K. Amine, Electrochim. Commun. 11 (2009) 1073.
- [8] Z. Chen, J.R. Dahn, Electrochim. Acta 49 (2004) 1079.
- [9] Y.S. Jung, A.S. Cavanagh, L.A. Riley, S.H. Kang, A.C. Dillon, M.D. Groner, S.M. George, S.H. Lee, Adv. Mater. 22 (2010) 2172.
- [10] B.J. Hwang, C.Y. Chen, M.Y. Cheng, R. Santhanam, K. Ragavendran, J. Power Sources 195 (2010) 4255.
- [11] W. Chang, J.W. Choi, J.C. Im, J.K. Lee, J. Power Sources 195 (2010) 320.
- [12] J. Cho, Y. Kim, B. Kim, J. Lee, B. Park, Angew. Chem., Int. Ed. 42 (2003) 1618.
- [13] Y. Sun, J. Han, S. Myung, S. Lee, K. Amine, Electrochim. Commun. 8 (2006) 821.
- [14] Y. Sun, S. Cho, S. Myung, K. Amine, J. Prakash, Electrochim. Acta 53 (2007) 1013.
- [15] J.H. Park, J.S. Kim, E.G. Shim, Y.T. Hong, Y.S. Lee, S.Y. Lee, Electrochim. Commun. 12 (2010) 1099.
- [16] J.H. Park, J.H. Cho, S.B. Kim, W.S. Kim, S.Y. Lee, S.Y. Lee, J. Mater. Chem. 22 (2012) 12574.
- [17] J.H. Cho, J.H. Park, M.H. Lee, H.K. Song, S.Y. Lee, Energy Environ. Sci. 5 (2012) 7124.
- [18] H.C. Liou, P.S. Ho, R. Stierman, Thin Solid Films 339 (1999) 68.
- [19] L.Y. Jiang, Y. Wang, T.S. Chung, X.Y. Qiao, J.Y. Lai, Prog. Polym. Sci. 34 (2009) 1135.
- [20] M.C. Choi, Y.K. Kim, C.S. Ha, Prog. Polym. Sci. 33 (2008) 581.
- [21] M.K. Aydinol, A.F. Kohan, G. Ceder, Phys. Rev. B 56 (1997) 1354.
- [22] I.D. Scott, Y.S. Jeong, A.S. Cavanagh, Y. Yan, A.C. Dillon, S.M. George, S.H. Lee, Nano Lett. 11 (2011) 414.
- [23] H.S. Jeong, J.H. Kim, S.Y. Lee, J. Mater. Chem. 20 (2010) 9180.
- [24] J.H. Cho, J.H. Park, J.H. Kim, S.Y. Lee, J. Mater. Chem. 21 (2011) 8192.
- [25] E.S. Choi, S.Y. Lee, J. Mater. Chem. 21 (2011) 14747.
- [26] J. Liu, A. Manthiram, J. Phys. Chem. C 113 (2009) 15073.
- [27] L.A. Riley, S.V. Atta, A.S. Cavanagh, Y. Tan, S.M. George, P. Liu, A.C. Dillon, S.H. Lee, J. Power Sources 196 (2011) 3317.